Analytica Chimica Acta 1183 (2021) 338989

Contents lists available at ScienceDirect

Analytica Chimica Acta

journal homepage: www.elsevier.com/locate/aca

A novel sensing platform for the determination of alkaline phosphatase based on SERS-fluorescent dual-mode signals

Wei Wang, Yue Zhang, Wei Zhang, Yibing Liu, Pinyi Ma**, Xinghua Wang, Ying Sun, Daqian Song*

College of Chemistry, Jilin Province Research Center for Engineering and Technology of Spectral Analytical Instruments, Jilin University, Qianjin Street 2699, Changchun, 130012, China

HIGHLIGHTS

- A sensing platform for alkaline phosphatase detection is developed based on SERS-fluorescent dual-mode signals.
- Dual-mode sensing platform is used to evaluate alkaline phosphatase inhibitor.
- Dual-mode sensing platforms can combine the advantages of SERS and fluorescence.
- The dual-mode sensing platform could be further applied to sense other diseases relating to alkaline phosphatase level.

GRAPHICAL ABSTRACT

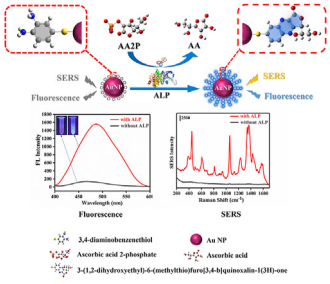

ARTICLE INFO

Article history:
Received 29 July 2021
Received in revised form
16 August 2021
Accepted 22 August 2021
Available online 25 August 2021

Keywords:
Alkaline phosphatase (ALP)
Fluorescence
Surface-enhanced Raman spectroscopy (SERS)
Dual-mode assay
Gold nanoparticles (AuNPs)

ABSTRACT

Alkaline phosphatase (ALP), as an important biomarker, is closely associated with various diseases. Multi-mode sensing platforms can combine the advantages of different technologies and solve their inherent or practical limitations. Herein, we developed a sensing platform for the determination of alkaline phosphatase (ALP) in human serum based on SERS-fluorescent dual-mode assay. Based on the fact that ALP can trigger the in-situ reaction between *o*-phenylenediamine (OPD) and ascorbic acid (AA), we connected gold nanoparticles (AuNPs) to 3,4-diaminobenzene-thiol (OPD(SH)) through an Au−S covalent bond to synthesize a nanoprobe (OPD(S)-AuNPs). The nanoprobe provides a unique interactive ammonium group for the diol group of AA, which was then used to generate an N-heterocyclic compound that can exhibit good SERS and fluorescence signals without adding SERS reporter and fluorophores or quantum dots (QDs). When being excited at different wavelengths as 360 nm and 785 nm, the fluorescence and SERS signals can be separately generated, which can avoid the disturbance from each other. The response of the fluorescence system was linear from 1.0 to 20 mU mL^{-1} ($R^2 = 0.994$) with a detection limit of 0.3 mU mL^{-1}, while that of the SERS system was linear from 0.5 to 10 mU mL^{-1} ($R^2 = 0.998$) with a detection limit of 0.2 mU mL^{-1}. The sensing platform developed was further employed in ALP inhibitor evaluation.

* Corresponding author.
** Corresponding author.
E-mail addresses: mapinyi@jlu.edu.cn (P. Ma), songdq@jlu.edu.cn (D. Song).

https://doi.org/10.1016/j.aca.2021.338989
0003-2670/

1. Introduction

Alkaline phosphatase (ALP) is a ubiquitous membrane-bound glycoprotein that can non-specifically catalyze the hydrolysis or dephosphorylation of various phosphoryl monoesters in alkaline media [1–4]. Abnormally elevated ALP levels are closely linked to many diseases, such as diabetes [5], liver insufficiency [6], bone diseases [7], hepatitis [8], and dynamic breast [9]. Abnormally reduced ALP levels are also associated with blood system diseases, such as Wilson's disease and leukemia [10,11]. Therefore, sensitive determination of ALP can play a significant role in the clinical diagnosis of ALP-related diseases. A variety of methods for the determination of ALP have been developed, such as capillary electrophoresis [12], electrochemical method [13], chromatography [14], colorimetry [15], and chemiluminescence method [16]. These methods have good accuracy and reproducibility in the determination of ALP, thus are sufficient for potentially applying in clinical trials. However, these methods also have limitations, as they require multi-step sample pretreatment, time-consuming fixation processes, laborious synthesis procedures, and complicated instruments, which have greatly limited their practical applications in the diagnosis of ALP-related diseases.

In recent years, fluorescence method that is convenient, fast and highly sensitive, and surface-enhanced Raman spectroscopy (SERS) that has high sensitivity and multiplexing capability in molecular-specific fingerprint spectroscopy, have been widely used in biological analysis [17–20]. However, the separate use of these two methods still suffers from some shortcomings. In fluorescence method, the organic fluorophores may lead to problems of photobleaching and quenching [21], while quantum dots (QDs) have problems such as in vivo toxic application and difficulty in surface modification [22]. Compared with fluorescence method, SERS method is still a low-throughput imaging technique that requires a longer acquisition time [23].

Therefore, SERS-fluorescent dual-mode sensing platform is a promising rapid and sensitive quantitative analysis tool, which has great potential in high-throughput multiplex analysis and biological imaging. By effectively integrating multiple functions on a sensing platform through multifunctional nanomaterials, the advantages of different technologies can be combined while solving their inherent or practical limitations. However, the SERS-fluorescent dual-mode sensing platform has some difficulties. For example, the construction of probes is complex, and requires the modification of organic fluorophores or QDs and SERS reporter on noble metal nanoparticles with surface plasmon effects [24]. The protective layer (Silica shell) is usually added on the modified metal surface to protect the fluorophores or QDs and SERS reporter from environmental influences [25,26]. Besides, when excitation laser in resonance with the electronic excitation of the fluorophores is used, the fluorescence signal can overshadow the resonance Raman signal, interfering with the detection of SERS in biological analysis [27].

In this study, we report a sensing platform for sensitive and selective assay of ALP activity by SERS-fluorescent dual-mode method. Gold nanoparticles (AuNPs) are often used as SERS substrates due to their unique optical and electrical properties [28]. Based on the fact that ALP can trigger the in-situ reaction of *o*-phenylenediamine (OPD) and ascorbic acid (AA), we synthesize a nanoprobe (OPD(S)-AuNPs) using an Au—S covalent bond to connect between 3,4-diaminobenzene-thiol (OPD(SH)) and AuNPs. The probe provides a unique interactive ammonium group for the diol group of AA to generate an N-heterocyclic compound that can exhibit good SERS and fluorescence signals without adding fluorophores or QDs and SERS reporter. When being excited at different wavelengths as 360 nm and 785 nm, the SERS and fluorescence signals can be separately generated, which can avoid the disturbance from each other. The enhancement of the SERS and fluorescence signals was found to be directly associated with the level of AA released from the ALP-triggered hydrolysis. Besides, the platform developed here was employed in ALP inhibitor evaluation.

2. Experimental section

2.1. Preparation of OPD(S)-AuNPs

AuNPs with a particle size of about 46 nm were synthesized according to the method previously reported [29]. Briefly, 50 μL of 0.1 g mL^{-1} $HAuCl_4$ solution was mixed with 50 mL of ultrapure water and then boiled. After that, 300 μL of sodium citrate solution (1 wt%) was quickly added into the boiling $HAuCl_4$ solution, which caused the solution color to change from light yellow to blue-black and finally to wine red. The mixture was then boiled for about 10 min before being cooled down to room temperature. The obtained AuNPs were centrifuged, resuspended in 50 mL of ultrapure water, and then stored at 4 °C until subsequent use. Then, 600 μL of OPD(SH) was added to 2 mL of the synthesized AuNPs solution, and the mixture was diluted to 3 mL with Tris-HCl buffer (50 mM, pH = 9). The mixture was vigorously shaken in the dark at room temperature for 30 min. The dual-readout nanoprobe (OPD(S)-AuNPs) was fabricated.

2.2. Determination of AA concentration

AA (100 μL) at concentrations from 0 to 200 μM was added into Tris-HCl buffer (400 μL, 50 mM, pH = 9.0). The mixture was mixed with 500 μL of OPD(S)-AuNPs solution. The resulting mixtures were stored in the dark for 30 min, and their photographs under 365 nm ultraviolet light were then taken before being subjected to fluorescence and SERS measurements.

2.3. Assaying ALP activity

ALP (100 μL) with activities from 0 to 200 mU mL^{-1} and 100 μL of AA2P (10 mM) was added into Tris-HCl buffer (300 μL, 5 mM, pH = 9) containing 5 μM $MgCl_2$. After incubating at 37 °C for 50 min, the mixture (500 μL) was mixed with 500 μL of OPD(S)-AuNPs solution. The resulting mixtures were kept in the dark for 30 min before their photographs under 365 nm ultraviolet light were taken; after that, they were subjected to fluorescence and SERS measurements.

2.4. Selectivity evaluation

Some potential interfering molecules, including K^+, Na^+, Ca^{2+}, Cl^-, trypsin, lysozyme, ACP, GOx, AChE, Glu, Tyr, BSA, Gly, and ATP, were used in the selectivity evaluation of the fluorescence method-based ALP assay. The influences of some ions, including Na^+, K^+, Ca^{2+}, and Cl^-, on SERS-based ALP assay were also assessed. The concentration of ALP used in these experiments was 200 mU mL^{-1}.

2.5. Assaying ALP activity in serum

Serum samples were centrifuged at 10000 rpm for 10 min at room temperature. The ALP with different activities used in section 2.4 was replaced with serum samples. The serum samples were diluted with ultra-pure water under the same conditions to ensure that the ALP level was within the same linear range as that of the above ALP activity assay.

2.6. Evaluation of ALP inhibitor

To evaluate the inhibitory effect of Na_3VO_4 on ALP, 50 μL of Na_3VO_4 aqueous solution at different concentrations (from 0 to 20 mM) was initially added into ALP aqueous solution (50 μL, 200 mU mL^{-1}) incubated in a 37 °C water bath. After 30 min, the Na_3VO_4-treated ALP and 100 μL of AA2P (20 mM) were added to Tris-HCl buffer (300 μL, 50 mM, pH = 9) containing 5 μM $MgCl_2$. The reaction solution was incubated at 37 °C for 50 min before being mixed with 500 μL of OPD(S)-AuNPs solution. The resulting mixtures were kept in the dark for 30 min, and their SERS and fluorescence signals were measured, respectively, to evaluate the inhibition effect of Na_3VO_4 on ALP.

3. Results and discussion

3.1. Specific optical reaction between OPD(S)-AuNPs and AA

OPD(SH) has a 1,2-diamine structure and can easily react with AA to form an N-heterocyclic compound (3-(1,2dihydroxyethyl)-6-(methylthio)furo[3,4-b] quinoxalin-1(3H)-one). The principle of the specific reaction between OPD(S)-AuNPs and AA is illustrated in Fig. 1A. According to a previous report, an N-heterocyclic compound is highly fluorescent [30]. Due to sulfur in its structure, OPD(SH) can be adsorbed onto the surface of AuNPs through an Au—S covalent bond. We found that the mixture solution of OPD(S)-AuNPs and AA exhibited an apparent emission peak at 480 nm when excited at 360 nm, generating a spectacularly intense blue emission under ultraviolet light (Fig. 1B). To verify that the fluorescence intensity obtained from this experiment was generated due to the quinoxaline derivative produced by AA and OPD(SH), we selected several substances that may emit fluorescence in the same solution and detected their fluorescence signals. Fig. S1 shows that in the absence of AA, AuNPs solution and OPD(S)-AuNPs solution did not exhibit fluorescence signals. After OPD(S)-AuNPs aqueous solution was incubated with AA, a clear emission peak appeared at about 480 nm. Besides, when the AuNPs solution was incubated with AA, the fluorescence intensity was still weak. These results prove that OPD(S)-AuNPs could react with AA, and the reaction generated specific fluorescence emission.

We chose the chemically synthesized AuNPs with a particle size of about 46 nm, as they generate high-intensity LSPR signal, to obtain SERS signals **(Fig. S2A).** OPD(SH) could be adsorbed onto the surface of AuNPs through an Au—S covalent bond, resulting in the synthesis of OPD(S)-AuNPs **(Fig. S2B)**. The UV—vis absorption spectra of AuNPs and OPD(S)-AuNPs are shown in Fig. S2**C**. As can be seen, the UV—visible absorption of AuNPs was around 532 nm; but after being modified with OPD(SH), the absorption was only slightly redshifted from 532 nm to 534 nm. And it can be seen in Fig. S2B that there is no obvious aggregation of OPD(S)-AuNPs. This indicates that the morphology of AuNPs both before and after modification was not changed and OPD(S)-AuNPs were successfully synthesized.

OPD(S)-AuNPs were selected as an SERS substrate to detect the concentration of AA. We found that in the absence of AA, AuNPs solution and OPD(S)-AuNPs solution exhibited very weak SERS signals. However, after OPD(S)-AuNPs solution was incubated with AA, the SERS intensity was enhanced, and the characteristic peaks appeared **(Fig. 1C)**. To reliably assign the SERS peaks, DFT calculations by Gaussian 16 program with B3LYP level of theory and

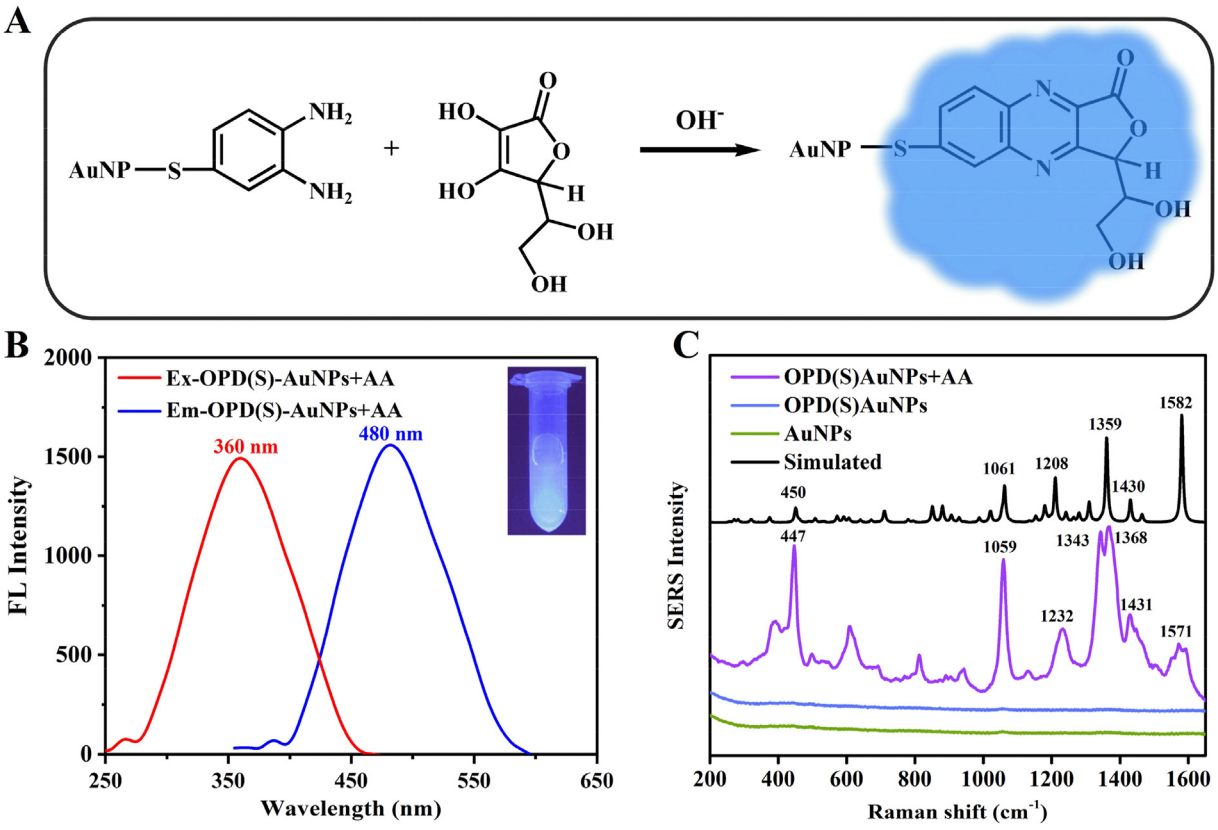

Fig. 1. (A) Schematic illustration of the reaction between OPD(S)-AuNPs and AA. **(B)** Fluorescence emission spectra of a mixture solution of OPD(S)-AuNPs with AA (Inset: the corresponding photographs captured under 365 nm ultraviolet light). **(C)** SERS spectra of AuNPs solution, OPD(S)-AuNPs solution, OPD(S)-AuNPs solution incubated with AA, and simulated SERS spectrum of OPD(S)-AuNPs solution incubated with AA.

6−311 + G (d, p) basis were conducted. The vibrational assignments are given in Table S1. Comparing the experimental SERS spectra with the simulated SERS spectrum of the product (Fig. 1C), we observed that most of the Raman vibrations were in good agreement with the experimental results. These results show that the specific reaction of OPD(S)-AuNPs and AA exhibited strong SERS signals.

3.2. ALP detection principle of the sensing platform

Based on the above principles, the SERS and fluorescence intensity before and after the addition of AA were obviously different. AA2P is one of the most frequently used substrates in the turn-on ALP activity assays, as it can be hydrolyzed and transformed into ascorbic acid (AA) [31,32], which is a molecule that lays a foundation for the determination of ALP activity by SERS and fluorescence methods.

We designed a sensing platform using OPD(S)-AuNPs as a nanoprobe for the determination of AA and ALP (Fig. 2). In the sensing platform, OPD(S)-AuNPs play dual roles. On the one hand, OPD(S)-AuNPs are also used as a fluorescence probe to form a quinoxaline fluorophore in the dephosphorylation of AA2P catalyzed by ALP and in the controllable in-situ fluorescence reaction with AA. On the other hand, OPD(S)-AuNPs not only serves as a SERS probe, but also provides a unique interactive ammonium group for the normal diol of AA, which is a compound used to generate N-heterocyclic compound that can exhibit good SERS signals. Based on the obvious difference between the signals generated before and after the addition of AA, we can expect the superior performance of our SERS and fluorescence methods in assaying AA and ALP.

3.3. Assays of AA by the sensing platform

Under the optimal experimental conditions, the calibration plots of the assay achieved using both the SERS system and the fluorescence system were constructed. The respective text and figures on the optimizations are given in the Electronic Supporting Material. The intensity of fluorescence was used to evaluate the performance of the proposed fluorescence system, where FL intensity represents the difference of the fluorescence intensity at 480 nm of the culture medium containing different concentrations of AA. The intensity of SERS was used to evaluate the performance of the proposed SERS sensor, where ΔI_{SERS} represents the difference of the SERS intensity at 1059 cm^{-1} of the culture medium containing different concentrations of AA.

As shown in Fig. 3A, the fluorescence intensity at 480 nm (excitation at 360 nm) gradually increased with increasing AA from 0 to 200 μM. The correlation had excellent linearity from 0.5 to 50 μM with a regression equation $y = 11.16x + 148.20$ (correlation coefficient $R^2 = 0.992$) (Fig. 3B). The limit of detection (LOD) was 0.21 μM (as calculated by 3σ/slope, where σ is the standard deviation of the blank samples). Additionally, the SERS intensity at 1059 cm^{-1} gradually increased with the increase of AA concentration in a range from 0 to 200 μM (Fig. 3C). The correlation had excellent linearity from 0.5 to 30 μM with a regression equation $y = 3146.11x + 45.65$ (correlation coefficient $R^2 = 0.994$) (Fig. 3D). The limit of detection (LOD) was 0.15 μM (calculated by 3σ/slope, where σ is the standard deviation of the blank samples). These results prove that OPD(S)-AuNPs can react with AA to generate N-heterocyclic compounds in an alkaline environment. The product not only can generate good SERS signals, but also can emit specific fluorescence signals. The good linear relationship under both SERS and fluorescence methods lays the foundation for ALP determination.

3.4. ALP activity assayed by the universal sensing platform

As designed, the intensity of fluorescence signal centered at 480 nm and that of SERS signal at 1059 cm^{-1} gradually increased with the increase of ALP activity, due to the increase of the AA2P hydrolysis and the concentration of AA produced.

The intensity of fluorescence signal at 480 nm, which was obtained after being excited at 360 nm, gradually increased with the increase of ALP activity in a range from 0 to 300 mU mL^{-1} (Fig. 4A). The correlation between the fluorescence intensity and ALP activity was linear from 1.0 to 20 mU mL^{-1} with a regression equation $y = 28.60\ x + 168.22$ (correlation coefficient $R^2 = 0.994$) (Fig. 4B). The limit of detection (LOD) calculated by 3σ/slope, where σ is the standard deviation of the blank samples, was 0.3 mU mL^{-1}. The SERS intensity at 1059 cm^{-1} gradually increased with the increase of ALP activity in a range from 0 to 200 mU mL^{-1} (Fig. 4C). The

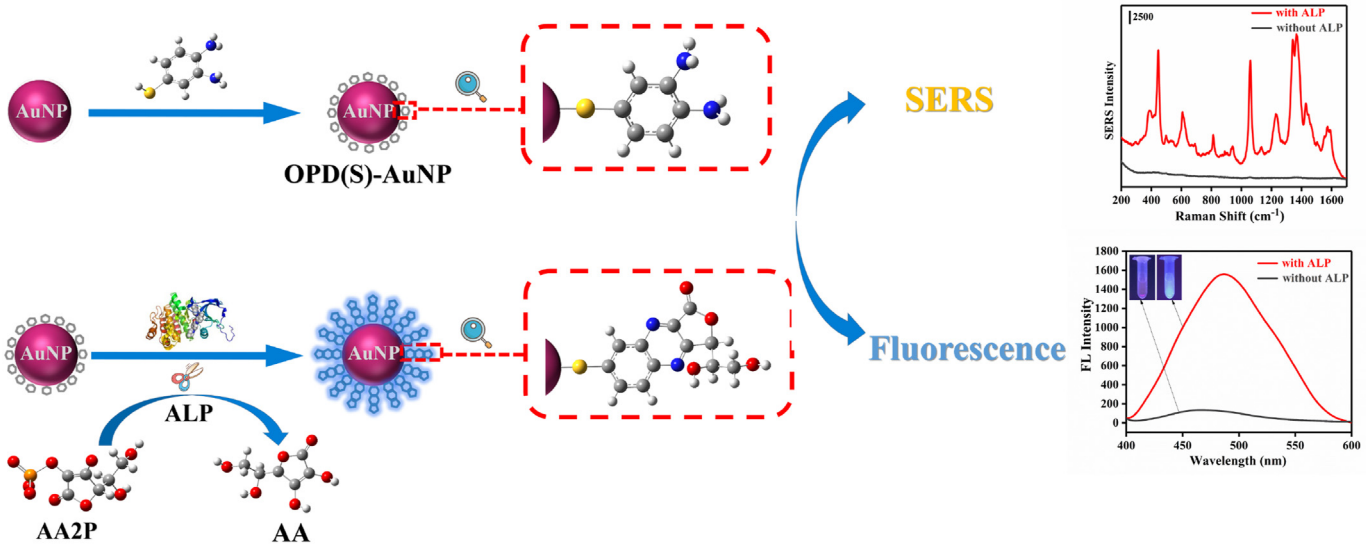

Fig. 2. Schematic illustration for the determination of ALP activity based on the ALP-triggered OPD(S)-AuNPs reaction with AA.

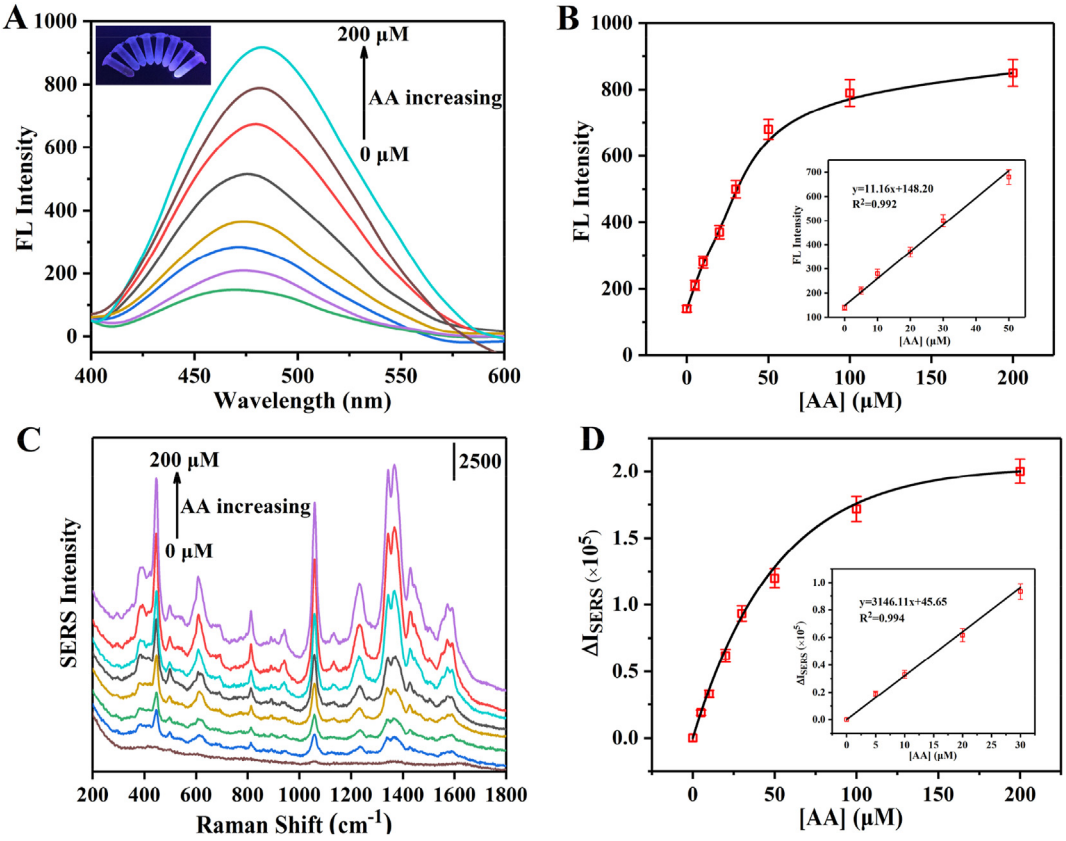

Fig. 3. (A) Fluorescence response of thesensing platform upon the addition of AA at various concentrations (Inset: the corresponding photographs captured under 365-nm ultraviolet light). (B) Plots of fluorescence intensity vs AA concentration. (C) SERS response of the sensing platform upon the addition of AA at various concentrations. (D) Plots of the difference of SERS intensity vs AA concentration.

correlation between the two was excellently linear from 0.5 to 10 mU mL^{-1} with a regression equation y = 1.77x + 22122.60 (correlation coefficient R^2 = 0.998) (Fig. 4D). The LOD calculated 3σ/slope was 0.2 mU mL^{-1}. These results indicate the good response and effectiveness of the sensing platform in the determination of ALP activity. We further compared ALP determination capability of our method with that of other reported methods, and the data are shown in Table 1. Compared with the single-mode systems, our sensing platform has a wider linear range and higher sensitivity. Furthermore, we compared other systems and found that the detection limit of our platform is similar to or lower than that of other methods, and only a few of these probes are based on both SERS and fluorescence methods.

3.5. Selectivity

Various interfering species, including several inorganic ions (K^+, Na^+, Ca^{2+}, and Cl^-), enzymes (trypsin, lysozyme, ACP, GOx, and AChE), and biomolecules (Glu, Tyr, BSA, Gly, and ATP), were used in this experiment. The concentration of K^+, Na^+, Ca^{2+}, Cl^-, Glu, Tyr, BSA, Gly, and ATP used was 10 mM, whereas that of trypsin, lysozyme, ACP, GOx, and AChE was 500 mU mL^{-1}. The results from the selectivity experiments are shown in Fig. 5. As shown, the incubation with the above interferences did not cause a remarkable signal change; and the apparent fluorescence change was observed only when ALP was introduced. This indicates that the fluorescence system has good selectivity toward ALP. Considering nanoparticle solution, the presence of ions at a high concentration may cause the imbalance of the surface charge of the nanoparticles, in turn causing them to aggregate, resulting in the decrease of their SERS activity. Thus, we also detected the influence of some ions, including Na^+, K^+, Ca^{2+}, and Cl^- (each at 10 mM), on ALP assay by the SERS method (Fig. 5B). The concentration of the interfering ions selected in the experiment exceeded that of the ions in diluted normal human serum [41]. These results show that both the fluorescence and SERS methods have high selectivity toward ALP.

3.6. ALP activity in serum obtained by the dual-mode sensing platform

Abnormal fluctuation of ALP activity in serum can be used as an important criterion for disease diagnosis, and the normal activity of ALP in human serum range from 40 to 190 mU mL^{-1} [42]. To demonstrate the applicability of the system in assaying real sample, ALP activity in real human serum sample was investigated. We diluted the human serum sample 10 times to ensure that the final ALP concentration in the sample remains within the linear measurement range. The results are illustrated in Fig. 6A. An ELISA calibration curve was constructed using ALP standard solution at concentrations ranging from 0 to 1000 mU mL^{-1}. The optical density at 450 nm was plotted against ALP concentration, as shown in Fig. 6B. Based on the plot, which was linear, the concentrations of ALP in human serum were calculated; and the results are given in Table 2. The results from the three methods were not significantly different, indicating the sensing platform could reliably assay ALP in the serum sample. Thus, it can be inferred that the system developed in this work is highly suitable for assaying ALP activity in clinical diagnosis.

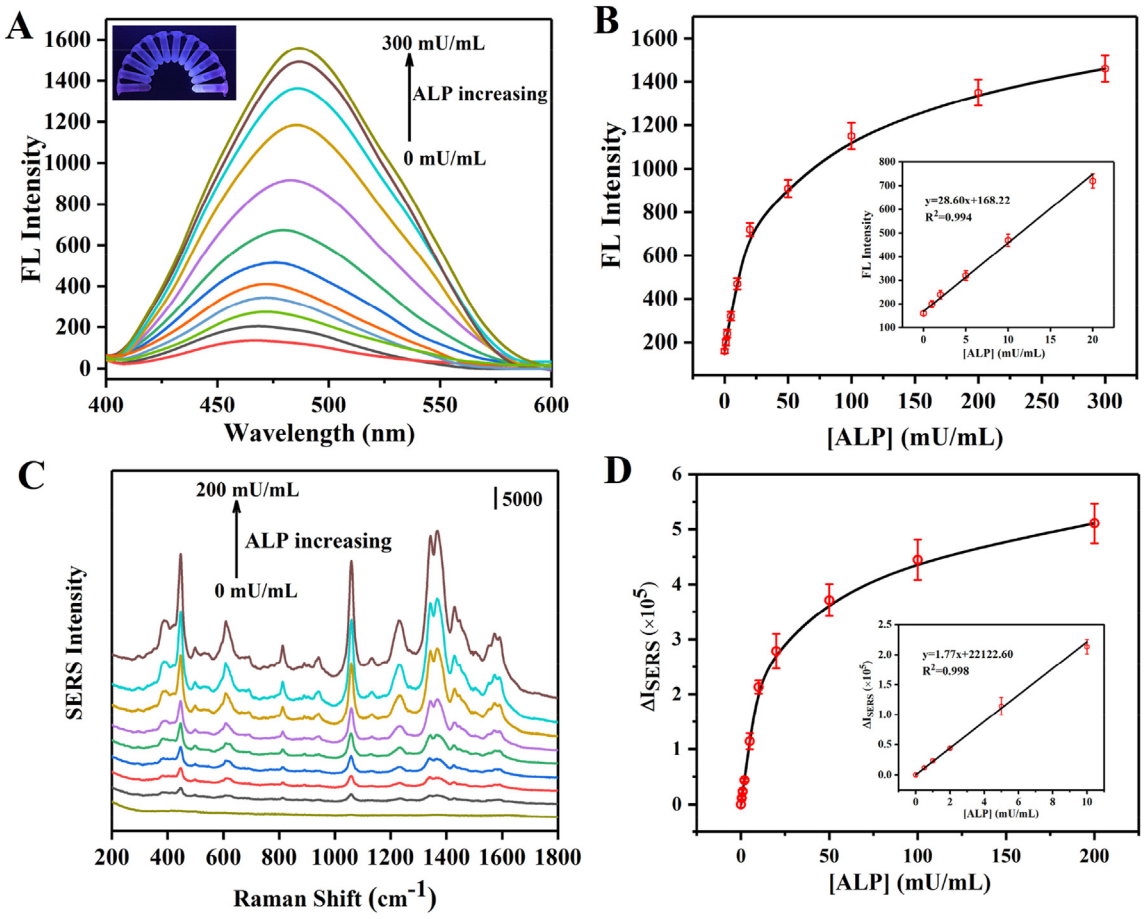

Fig. 4. (A) Fluorescence response of the sensing platform upon the addition of ALP with various activities (Inset: the corresponding photographs captured under 365-nm ultraviolet light). (B) Plots of fluorescence intensity vs ALP activity. (C) SERS response of the sensing platform upon the addition of ALP with various activities. (D) Plots of the difference of SERS intensity vs ALP activity.

3.7. Screening of ALP inhibitor

To confirm its effectiveness, our sensing platform was employed to screen ALP inhibitors. Na_3VO_4 is a common ALP inhibitor that has been used in various inhibitor screening experiments [43]. The half-maximal inhibitory concentration (IC_{50}), which is the concentration of an inhibitor required to inhibit 50% of an enzyme, was used as a parameter to evaluate the inhibitor used in this study.

With increasing Na_3VO_4 concentration and a constant ALP activity (200 mU mL^{-1}), the fluorescence (Fig. 7A) and SERS (Fig. 7C) intensity decreased in a concentration-dependent manner, clearly demonstrating Na_3VO_4 could exert its inhibitory effect on ALP. As depicted in Fig. 7B and **D**, the plots between fluorescence intensity and ΔI_{SERS} value versus log Na_3VO_4 concentration had a sigmoidal pattern. The IC_{50} values of the inhibitor against 200 mU mL^{-1} ALP detected by the fluorescence system and the SERS system were

Table 1
Comparison of the developed method for the determination of ALP with other reported methods.

Method	Materials	Mode	Determination of ALP		Ref.
			Linear range (mU mL^{-1})	Detection limit (mU mL^{-1})	
Single-mode	G_{20}–Cu(II)	Colorimetry	20–200	0.84	[33]
	UC NPs	Luminescence	62.5–87.5	19	[34]
	DNA/AgNCs	Fluorescence	30–0.24	5	[35]
	Au NR@Ag	Colorimetry	5–100	3.3	[15]
	hemicyanine	Fluorescence	10–2000	3	[36]
Dual-mode	CoOOH	Fluorescence	0.04–160	0.026	[37]
		Colorimetry	0.04–160	0.032	
	PAPP	Fluorescence	0.1–40	0.03	[38]
		Colorimetry	0.2–100	–	
	4-MPBA-Au@Ag NPs	SERS	0.5–10	0.10	[39]
		Colorimetry	–	5.0	
	Au-NPs@GMP-Tb	Fluorescence	0–400	0.4	[40]
		Colorimetry	5–400	1.2	
	OPD(S)-AuNPs	SERS	0.5–10	0.2	This work
		Fluorescence	1.0–20	0.3	

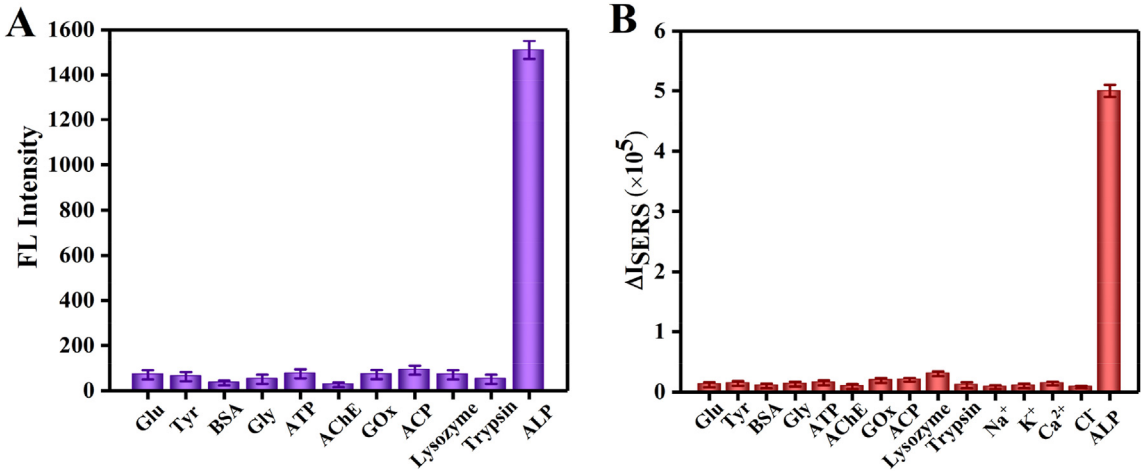

Fig. 5. Fluorescence intensity (A) and SERS intensity (B) of OPD(S)-AuNPs solution incubated with ALP (200 mU mL^{-1}) or various interferences.

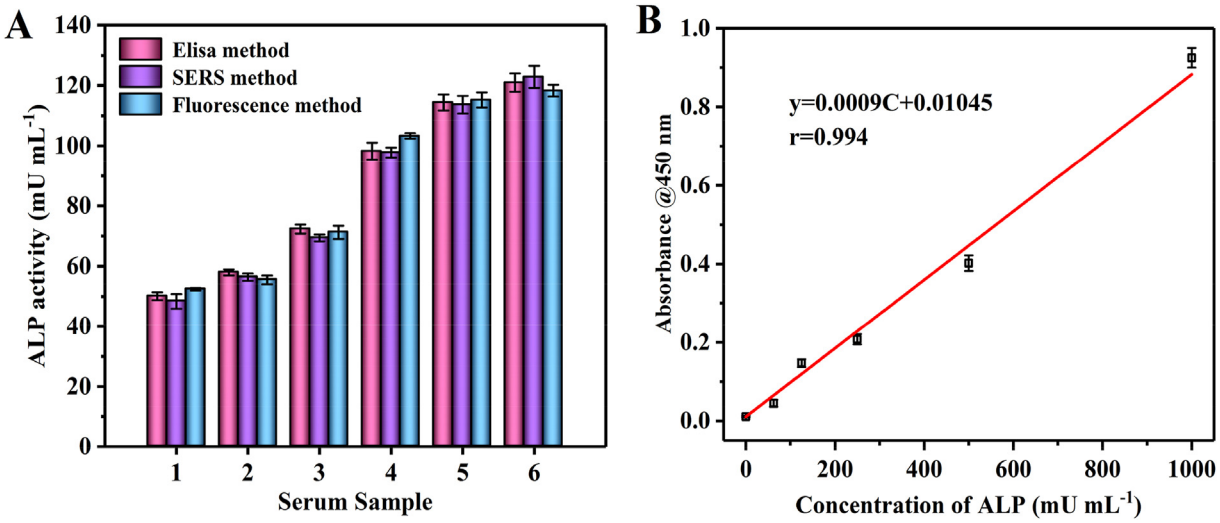

Fig. 6. (A) Comparison of ALP activities in real human serum samples obtained by the proposed assay and a commercial reagent kit. (B) Standard curve of ALP constructed by ELISA.

Table 2
Results for clinical serum samples obtained from the sensing platform and the ELISA method (n = 3).

Samples	Elisa Result (mU mL^{-1})	SERS Result		Fluorescence Result	
		Detection level (mU mL^{-1})	Relative error (%)	Detection level (mU mL^{-1})	Relative error (%)
1	50.02 ± 1.34	48.32 ± 2.44	96.60	52.36 ± 0.45	104.68
2	57.94 ± 0.99	56.37 ± 1.21	97.29	55.45 ± 1.45	95.70
3	72.34 ± 1.52	69.38 ± 1.12	96.91	71.21 ± 2.21	98.44
4	98.20 ± 2.84	97.75 ± 1.65	99.54	103.27 ± 0.88	105.16
5	114.38 ± 2.65	113.66 ± 2.95	99.37	115.23 ± 2.49	100.74
6	120.98 ± 3.02	122.89 ± 3.63	101.58	118.28 ± 1.97	97.77

2.097 mM and 1.984 mM, respectively, which are consistent with the values reported previously [44]. These results essentially demonstrate that the sensing platform developed in this study, which used OPD(S)-AuNPs as the nanoprobe, could also evaluate the effect of inhibitor on an enzyme.

4. Conclusion

In summary, a fluorescence-SERS dual-mode sensing platform for determination of ALP activity and screening ALP inhibitors was successfully developed. Based on the fact that ALP can trigger the in situ reaction between 3,4-diaminobenzene-thiol and ascorbic acid, a nanoprobe was synthesized from gold nanoparticles and 3,4-diaminobenzene-thiol connected through an Au—S covalent bond. The enhancement of SERS and fluorescence signals may be the result of the diol group of AA, N-heterocyclic compounds generated from the reaction between the ketone group of AA and the 1,2-diamine group in benzenethiol. The constructed sensing platform can applied to the fluorescence and SERS system which had high selectivity and sensitivity with remarkable LODs of 0.3 mU mL^{-1} and 0.2

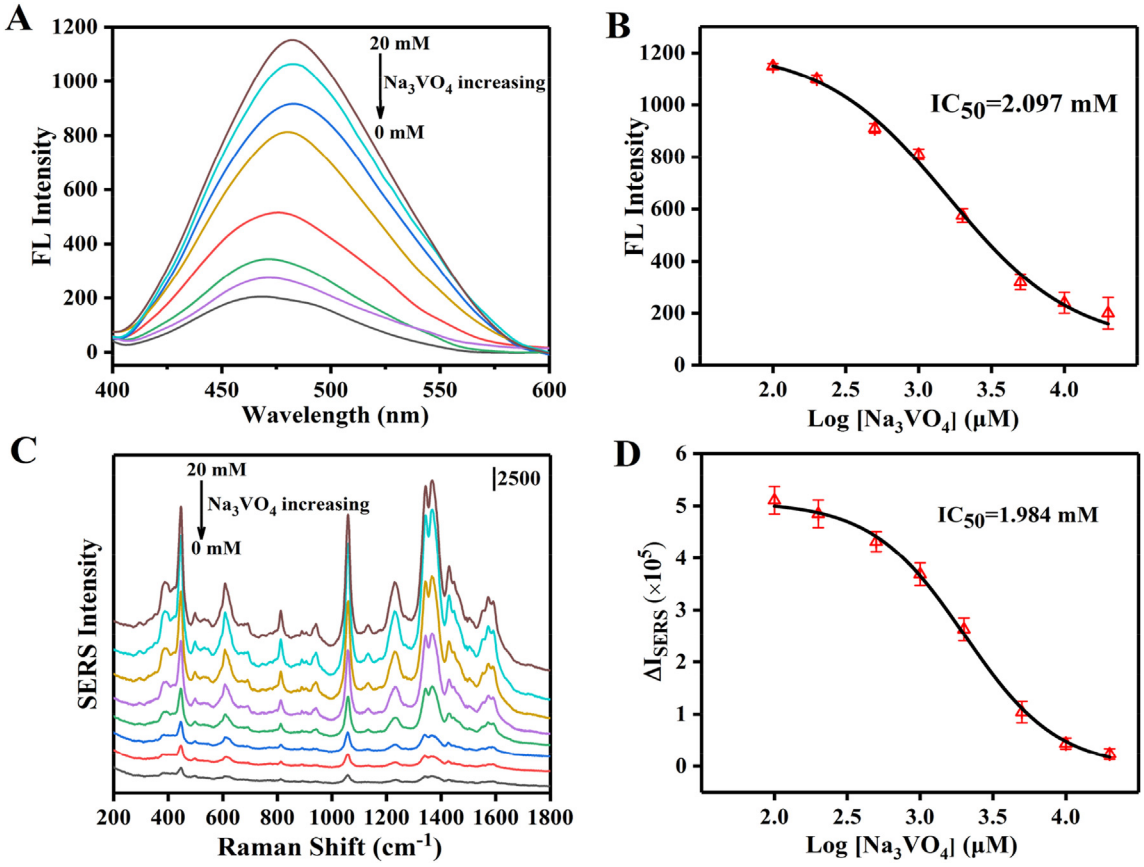

Fig. 7. Effect of inhibitor on ALP evaluated by the sensing platform. (A) Fluorescence spectra of Na_3VO_4-treated ALP with increasing concentration from 0 to 20 mM. (B) Plot of fluorescence intensity versus log Na_3VO_4 concentration. (C) SERS spectra of Na_3VO_4-treated ALP with increasing concentration from 0 to 20 mM. (D) Plot of ΔI_{SERS} value versus log Na_3VO_4 concentration. Error bars indicate standard deviations (n = 3).

mU mL^{-1}, respectively. In the sensing platform of diluted human serum sample, excellent recoveries between 95.70% and 104.76% were obtained, indicating the method could promisingly be applied to assay biological samples. The dual-mode sensing platform is efficient and simple without adding fluorophores or QDs and SERS reporter. Under different wavelength excitations, SERS and fluorescence signals can be generated separately, avoiding mutual interference. The sensing platform is a promising tool that should be applied in the diagnosis of various ALP-related diseases.

CRediT authors contribution statement

Wei Wang: Conceptualization, Methodology, Software, Investigation, Validation, Data curation, Writing-original draft. Yue Zhang: Data analysis, Writing-review & editing. Wei Zhang: Resources, Data analysis & Validation. Yibing Liu: Writing-review & editing. Pinyi Ma: Conceptualization, Project administration, Data curation, Writing-review. Xinghua Wang: Investigation, Supervision. Ying Sun: Data curation. Daqian Song: Project administration, Funding acquisition, Resources, Supervision.

CRediT authorship contribution statement

Wei Wang: Conceptualization, Methodology, Software, Investigation, Validation, Data curation, Writing – original draft. **Yue Zhang:** Formal analysis, Writing – review & editing. **Wei Zhang:** Resources, Formal analysis, Validation. **Yibing Liu:** Writing – review & editing. **Pinyi Ma:** Conceptualization, Project administration, Data curation, Writing – review & editing, Writing-review. **Xinghua Wang:** Investigation, Supervision. **Ying Sun:** Data curation. **Daqian Song:** Project administration, Funding acquisition, Resources, Supervision.

Declaration of competing interest

The authors declare that they have no known competing financial interests or personal relationships that could have appeared to influence the work reported in this paper.

Acknowledgments

This work was supported by the National Natural Science Foundation of China(Grant Nos. 22074052 and 22004046).

Appendix A. Supplementary data

Supplementary data to this article can be found online at https://doi.org/10.1016/j.aca.2021.338989.

References

[1] P.J. Butterworth, Alkaline phosphatase. Biochemistry of mammalian alkaline phosphatases, Cell Biochem. Funct. 1 (1983) 66–70.
[2] R.P. Cox, P. Gilbert Jr., M.J. Griffin, Alkaline inorganic pyrophosphatase activity of mammalian-cell alkaline phosphatase, Biochem. J. 105 (1967) 155–161.
[3] D.J. Goldstein, H. Harris, Mammalian brain alkaline phosphatase: expression of liver/bone/kidney locus. Comparison of fetal and adult activities, J. Neurochem. 36 (1981) 53–57.

[4] B. Lorenz, H.C. Schroder, Mammalian intestinal alkaline phosphatase acts as highly active exopolyphosphatase, Biochim. Biophys. Acta Protein Struct. Mol. Enzymol. 1547 (2001) 254–261.
[5] S.A.G. Kemink, A. Hermus, L. Swinkels, J.A. Lutterman, A.G.H. Smals, Osteopenia in insulin-dependent diabetes mellitus; prevalence and aspects of pathophysiology, J. Endocrinol. Invest. 23 (2000) 295–303.
[6] M. Yamazoe, A. Mizuno, Y. Nishi, K. Niwa, M. Isobe, Serum alkaline phosphatase as a predictor of worsening renal function in patients with acute decompensated heart failure, J. Cardiol. 67 (2016) 412–417.
[7] P. Magnusson, M.W.J. Davie, C.A. Sharp, Circulating and tissue-derived isoforms of bone alkaline phosphatase in Paget's disease of bone, Scand. J. Clin. Lab. Invest. 70 (2010) 128–135.
[8] X.-Z. Wu, D. Chen, L.-S. Zhao, X.-H. Yu, M. Wei, Y. Zhao, et al., Early diagnosis of bacterial and fungal infection in chronic cholestatic hepatitis B, World J. Gastroenterol. 10 (2004) 2228–2231.
[9] L.F.A. Wymenga, K. Groenier, J. Schuurman, J.H.B. Boomsma, R.O. Elferink, H.J.A. Mensink, Pretreatment levels of urinary deoxypyridinoline as a potential marker in patients with prostate cancer with or without bone metastasis, BJU Int. 88 (2001) 231–235.
[10] L. Liu, Q. Gong, J. Liu, H. Shen, H. Zhang, Y. Xue, Plasma transfusion combined with chelating therapy alleviates fulminant Wilson's disease with a single Arg778Leu heterozygote mutation, Ann. Hepatol. 18 (2019) 393–396.
[11] T. Stokol, D.M. Schaefer, M. Shuman, N. Belcher, L. Dong, Alkaline phosphatase is a useful cytochemical marker for the diagnosis of acute myelomonocytic and monocytic leukemia in the dog, Vet. Clin. Pathol. 44 (2015) 79–93.
[12] X.M. Sun, D. Li, Z.L. Bai, W.R. Jin, Electrochemical detection of alkaline phosphatase in BALB/c mouse fetal liver stromal cells with capillary electrophoresis, Chin. Chem. Lett. 15 (2004) 212–213.
[13] A. Kokado, H. Arakawa, M. Maeda, New electrochemical assay of alkaline phosphatase using ascorbic acid 2-phosphate and its application to enzyme immunoassay, Anal. Chim. Acta 407 (2000) 119–125.
[14] M.A. Cervinski, H.K. Lee, I.W. Martin, D.K. Gavrilov, A macro-enzyme cause of an isolated increase of alkaline phosphatase, Clin. Chim. Acta 440 (2015) 169–171.
[15] C.M. Li, S.J. Zhen, J. Wang, Y.F. Li, C.Z. Huang, A gold nanoparticles-based colorimetric assay for alkaline phosphatase detection with tunable dynamic range, Biosens. Bioelectron. 43 (2013) 366–371.
[16] L.X. Zhao, J.M. Lin, Z.J. Li, X.T. Ying, Development of a highly sensitive, second antibody format chemiluminescence enzyme immunoassay for the determination of 17 beta-estradiol in wastewater, Anal. Chim. Acta 558 (2006) 290–295.
[17] L. Ruiyi, J. Yanhong, W. Qinsheng, Y. Yongqiang, L. Nana, S. Xiulan, et al., Serine and histidine-functionalized graphene quantum dot with unique double fluorescence emission as a fluorescent probe for highly sensitive detection of carbendazim, Sensor. Actuator. B Chem. 343 (2021) 130099.
[18] C. Wang, X. Yang, S. Zheng, X. Cheng, R. Xiao, Q. Li, et al., Development of an ultrasensitive fluorescent immunochromatographic assay based on multilayer quantum dot nanobead for simultaneous detection of SARS-CoV-2 antigen and influenza A virus, Sensor. Actuator. B Chem. 345 (2021) 130372.
[19] H. Li, Y. Li, D. Wang, J. Wang, J. Zhang, W. Jiang, et al., Synthesis of hydrophilic SERS-imprinted membrane based on graft polymerization for selective detection of L-tyrosine, Sensor. Actuator. B Chem. 340 (2021) 129955.
[20] X. Wang, J. Zeng, Q. Sun, J. Yang, Y. Xiao, Z. Zhuo, et al., An effective method towards label-free detection of antibiotics by surface-enhanced Raman spectroscopy in human serum, Sensor. Actuator. B Chem. 343 (2021) 130084.
[21] J.V. Pellegrotti, G.P. Acuna, A. Puchkova, P. Holzmeister, A. Gietl, B. Lalkens, et al., Controlled reduction of photobleaching in DNA origami-gold nanoparticle hybrids, Nano Lett. 14 (2014) 2831–2836.
[22] Q. Zhang, Y. Sun, M. Liu, Y. Liu, Selective detection of Fe^{3+} ions based on fluorescence MXene quantum dots via a mechanism integrating electron transfer and inner filter effect, Nanoscale 12 (2020) 1826–1832.
[23] M. Li, J. Xu, M. Romero-Gonzalez, S.A. Banwart, W.E. Huang, Single cell Raman spectroscopy for cell sorting and imaging, Curr. Opin. Biotechnol. 23 (2012) 56–63.
[24] Y. Wang, L. Chen, P. Liu, Biocompatible triplex $Ag@SiO_2@mTiO_2$ core-shell nanoparticles for simultaneous fluorescence-SERS bimodal imaging and drug delivery, Chem. Eur J. 18 (2012) 5935–5943.
[25] X. Zhang, X. Du, Carbon nanodot-decorated $Ag@SiO_2$ nanoparticles for fluorescence and surface-enhanced Raman scattering immunoassays, ACS Appl. Mater. Interfaces 8 (2016) 1033–1040.
[26] Z. Wang, S. Zong, H. Chen, H. Wu, Y. Cui, Silica coated gold nanoaggregates prepared by reverse microemulsion method: dual mode probes for multiplex immunoassay using SERS and fluorescence, Talanta 86 (2011) 170–177.
[27] H.I. Khan, M.U. Khalid, A. Abdullah, A. Ali, A.S. Bhatti, S.U. Khan, et al., Facile synthesis of gold nanostars over a wide size range and their excellent surface enhanced Raman scattering and fluorescence quenching properties, J. Vac. Sci. Technol., B: Nanotechnol. Microelectron.: Mater., Process., Meas., Phenom. 36 (2018).
[28] C.E. Talley, J.B. Jackson, C. Oubre, N.K. Grady, C.W. Hollars, S.M. Lane, et al., Surface-enhanced Raman scattering from individual Au nanoparticles and nanoparticle dimer substrates, Nano Lett. 5 (2005) 1569–1574.
[29] X. Ji, X. Song, J. Li, Y. Bai, W. Yang, X. Peng, Size control of gold nanocrystals in citrate reduction: the third role of citrate, J. Am. Chem. Soc. 129 (2007) 13939–13948.
[30] Q. Yang, C. Li, J. Li, M. Arabi, X. Wang, H. Peng, et al., Multi-emitting fluorescence sensor of MnO_2-OPD-QD for the multiplex and visual detection of ascorbic acid and alkaline phosphatase, J. Mater. Chem. C 8 (2020) 5554–5561.
[31] S. Zhu, C. Lei, Y. Gao, J. Sun, H. Peng, H. Gao, et al., Simple and label-free fluorescence detection of ascorbic acid in rat brain microdialysates in the presence of catecholamines, New J. Chem. 42 (2018) 3851–3856.
[32] C. Liu, B. Ding, C. Xue, Y. Tian, G. Hu, J. Su, Sheathless focusing and separation of diverse nanoparticles in viscoelastic solutions with minimized shear thinning, Anal. Chem. 88 (2016) 12547–12553.
[33] J. Yang, L. Zheng, Y. Wang, W. Li, J. Zhang, J. Gu, et al., Guanine-rich DNA-based peroxidase mimetics for colorimetric assays of alkaline phosphatase, Biosens. Bioelectron. 77 (2016) 549–556.
[34] F. Wang, C. Zhang, Q. Xue, H. Li, Y. Xian, Label-free upconversion nanoparticles-based fluorescent probes for sequential sensing of Cu^{2+}, pyrophosphate and alkaline phosphatase activity, Biosens. Bioelectron. 95 (2017) 21–26.
[35] J.-L. Ma, B.-C. Yin, X. Wu, B.-C. Ye, Copper-mediated DNA-scaffolded silver nanocluster on-off switch for detection of pyrophosphate and alkaline phosphatase, Anal. Chem. 88 (2016) 9219, 9125.
[36] S.-J. Li, C.-Y. Li, Y.-F. Li, J. Fei, P. Wu, B. Yang, et al., Facile and sensitive near-infrared fluorescence probe for the detection of endogenous alkaline phosphatase activity in vivo, Anal. Chem. 89 (2017) 6854–6860.
[37] S.G. Liu, L. Han, N. Li, N. Xiao, Y.J. Ju, N.B. Li, et al., A fluorescence and colorimetric dual-mode assay of alkaline phosphatase activity via destroying oxidase-like CoOOH nanoflakes, J. Mater. Chem. B 6 (2018) 2843–2850.
[38] J. Zhao, S. Wang, S. Lu, X. Bao, J. Sun, X. Yang, An enzyme cascade-triggered fluorogenic and chromogenic reaction applied in enzyme activity assay and immunoassay, Anal. Chem. 90 (2018) 7754–7760.
[39] J. Zhang, L. He, X. Zhang, J. Wang, L. Yang, B. Liu, et al., Colorimetric and SERS dual-readout for assaying alkaline phosphatase activity by ascorbic acid induced aggregation of Ag coated Au nanoparticles, Sensor. Actuator. B Chem. 253 (2017) 839–845.
[40] X. Zhang, J. Deng, Y. Xue, G. Shi, T. Zhou, Stimulus response of Au-NPs@GMP-Tb core-shell nanoparticles: toward colorimetric and fluorescent dual-mode sensing of alkaline phosphatase activity in algal blooms of a freshwater lake, Environ. Sci. Technol. 50 (2016) 847–855.
[41] N. Agarwal, J.T. Prchal, Anemia of chronic disease (anemia of inflammation), Acta Haematol. 122 (2009) 103–108.
[42] D.D. Deligianni, N.D. Katsala, P.G. Koutsoukos, Y.F. Missirlis, Effect of surface roughness of hydroxyapatite on human bone marrow cell adhesion, proliferation, differentiation and detachment strength, Biomaterials 22 (2001) 87–96.
[43] J.-H. Lin, Y.-C. Yang, Y.-C. Shih, S.-Y. Hung, C.-Y. Lu, W.-L. Tseng, Photoinduced electron transfer between Fe(III) and adenosine triphosphate-BODIPY conjugates: application to alkaline-phosphatase-linked immunoassay, Biosens. Bioelectron. 77 (2016) 242–248.
[44] J. Deng, P. Yu, Y. Wang, L. Mao, Real-time ratiometric fluorescent assay for alkaline phosphatase activity with stimulus responsive infinite coordination polymer nanoparticles, Anal. Chem. 87 (2015) 3080–3086.